Available online at www.sciencedirect.com
ScienceDirect
Colloids and Surfaces A: Physicochem. Eng. Aspects 294 (2007) 254–266
COLLOIDS AND SURFACES A
www.elsevier.com/locate/colsurfa

Effect of electrostatic interaction on deposition of colloid on partially covered surfaces Part I. Model formulation

Paweł Weroński [a,b,*]

[a] *Institute of Catalysis and Surface Chemistry, Polish Academy of Sciences, ul. Niezapominajek 8, 30-239 Kraków, Poland*
[b] *Center for Nonlinear Studies and Theoretical Division, Los Alamos National Laboratory, MS-B284, Los Alamos, NM 87545, USA*

Received 26 July 2006; accepted 8 August 2006
Available online 15 August 2006

Abstract

We discuss the existing 2D and 3D random sequential adsorption (RSA) models and demonstrate that some of the assumptions used in these models can lead to incorrect results. Specifically, neglecting the particle–surface interaction at a distance from the adsorption surface in the 2D model can result in overestimating the surface blocking effect, while the assumption of the rectilinear particle trajectory in the model 3D can lead to inaccurate pair correlation functions. Next, we propose a new RSA approach that overcomes these shortcomings of the 2D and 3D models and allows modeling soft colloidal particle deposition (irreversible adsorption) on surfaces precovered with smaller particles. This approximate model allowing electrostatic interaction of colloid particles at a charged interface employs a many-body superposition approximation and considers adsorbing particle curvilinear trajectory in the thin electrolyte layer adjacent to the interface. Finally, we derive approximate analytical expressions for the available surface function of the adsorbing particle in the limit of low surface coverage, applying the 2D scaled-particle theory with a modification for the sphere geometry and electrostatic interaction.

Keywords: Adsorption of colloid particles; Particle electrostatic interaction; Colloid deposition; Monte Carlo simulation; Random sequential adsorption; RSA model

1. Introduction

The adsorption and deposition (irreversible adsorption) of colloids and bioparticles at solid/liquid interfaces are of great significance in many natural and practical processes such as water and wastewater filtration, membrane filtration, papermaking, flotation, protein and cell separation, enzyme immobilization, membrane biofouling, and artificial organ transplant. Often in these processes, especially in filtration, polydisperse suspensions or mixtures appear, e.g., colloid/polymer, colloid/macroscopic particle, or protein/surfactant. As a result of their higher diffusivity, the smaller components of the mixture will adsorb preferentially at the interface, forming a layer that may prohibit consecutive deposition of larger particles. This effect leads to a considerable decrease in the kinetics of larger-particle accumulation at the interface, as reported in the literature [1–3]. Similar problems often appear in model experiments concerned with protein or colloid–particle adsorption when the usual substrate cleaning procedure may produce a nanosized contaminant layer difficult to detect by conventional means. In respect to both charge distribution and geometry, formation of such a layer will produce surface heterogeneity, which is expected to influence the kinetics and maximum coverage of the adsorption experiments. Thus, modeling of adsorption phenomena at precovered surfaces seems an important and challenging task that can be accomplished using a variety of approaches. Among them, the random sequential adsorption (RSA) approach seems to be the most suitable one because of its simplicity and efficiency.

The classical RSA model considers a sequence of trials of particle adsorption on a homogeneous interface [4–6]. Once an empty surface element is found, the particle is permanently fixed, with no consecutive motion allowed. Otherwise, the virtual particle is rejected and a next-addition attempt is undertaken. Since the 1980s a number of extended RSA models have been developed that include the effects of particle

* Tel.: +1 505 667 9956; fax: +1 505 665 2659.
E-mail address: pawel@lanl.gov.

0927-7757/$ – see front matter © 2006 Elsevier B.V. All rights reserved.
doi:10.1016/j.colsurfa.2006.08.018

shape [7–11], Brownian motion [12–15], external force [16–19], particle–particle [20–22] and particle–interface [23] electrostatic interaction, colloid–particle polydispersity [24–26], and surface heterogeneity [27–30]. The results based on RSA simulations allow us to predict particle monolayer structure and the jamming coverage of particles. One may use the model to predict particle-adsorption kinetics as well, although depending on the particle-transport mechanism, an appropriate analysis of real adsorption problems can require inclusion of a correction for bulk transport or the hydrodynamic scattering effect [31]. Thus, RSA modeling can be a powerful tool in the study of irreversible adsorption of macromolecules, proteins, and colloid particles.

As discussed in this paper, however, both 2D and 3D RSA models that consider the effects of electrostatic interaction, often exploited for the interpretation of experimental results, are greatly simplified, and their application to bimodal systems can result in incorrect predictions. Therefore, the goal of this paper is to propose a new, more realistic adsorption approach. After a short discussion of the two existing models, we present the new curvilinear trajectory (CT) RSA approach of particle adsorption that includes the electrostatic interaction at the adsorption surface. We also derive approximate analytical expressions for the available surface function of the adsorbing particle in the limit of low surface coverage, applying the 2D scaled-particle theory with a modification for the sphere geometry and electrostatic interaction.

2. General considerations

We will describe particle deposition at heterogeneous surfaces using the two-stage RSA model exploited in our earlier studies [3,27,28,32,33], extended by including particle energy considerations as described later on. First, the heterogeneous surface is produced by covering a homogeneous interface with N_s small spherical particles of radius a_s. (In what follows, the subscripts s and l will always refer to small and large particles, respectively.) Then, adsorption of the larger particles (having a radius a_l) at such prepared random surface can be simulated. At both stages the number of adsorbed particles can be expressed in terms of dimensionless surface coverage defined as:

$$\theta_i = \frac{\pi a_i^2 N_i}{S}, \quad i = s, l, \tag{1}$$

where S is the geometrical area of the interface.

The particle adsorption probability B_i, called available surface function or blocking parameter, can be calculated for a given coverage θ_s and θ_l using the method of Schaaf and Talbot [5] by exploiting the definition:

$$B_i(\theta_s, \theta_l) = \frac{N^0_{\mathrm{succ}}}{N^0_{\mathrm{att}}}, \quad i = s, l, \tag{2}$$

where N^0_{att} and N^0_{succ} are the overall and successful number of adsorption attempts, respectively, performed at fixed θ_s and θ_l.

Obviously, at both deposition stages the particle–particle interaction and particle–interface interaction play a crucial role, influencing the kinetic and structural aspects of adsorption. Unfortunately, an exact determination of the interaction energy between particles near the adsorption surface in a general case seems prohibitive because of the inherent many-body problem. However, as demonstrated in Ref. [23], in the case of short-ranged interactions and not very low surface potentials, the van der Waals attraction is negligible, and the superposition approximation of the electrostatic interaction offers satisfactory accuracy of the total particle potential at the collector surface. Even with this simplification, including electrostatic interaction in the RSA model of adsorption at precovered surfaces is not an easy task. It should be remembered that RSA simulations exploit a Monte Carlo technique, which is strictly suitable for systems at equilibrium. Extending the technique to model transport-related or irreversible phenomena should carefully be considered to avoid unrealistic or unreasonable results. In the following sections, we discuss the three extended RSA models including electrostatic interaction. In what follows we assume constant potentials on all surfaces.

3. 2D model

Historically, the first model of RSA allowing electrostatic interaction among colloid particles was proposed by Adamczyk et al. [20] and is known as the 2D RSA model. This model neglects the particle transport from the bulk, assumes the perfect sink particle–interface interaction, and adopts the Monte Carlo method of calculating the adsorption probability. It exploits the Boltzmann distribution for the interparticle potential and takes into account only the lateral electrostatic interaction force. The interaction energy is calculated according to the linear superposition approximation (LSA) [34], with a dimensionless coefficient α accounting for the interface effect on the particle–particle lateral interaction, which is expected to be on the order of 0.5. Physically, this means that in the 2D model, the lateral repulsion of adsorbing particles is decreased by a half because of the overlapping of the particles' electric double layers and the double layer originating from the adsorption surface. For two spherical particles with radii a_i and a_j, separated by the gap width $H_1 = h_1/a_i$, expressed in particle radii a_i, the repulsive energy in the kT units is equal to:

$$E_{ij}(H_1) = \alpha\varepsilon\frac{kT}{e^2}Y_iY_j\frac{a_j}{1 + a_j/a_i + H_1}\exp(-\kappa a_i H_1), \quad i, j = l, s, \tag{3}$$

where ε is the dielectric constant of the medium, e the electron charge, $\kappa^{-1} = \sqrt{10^3\,\varepsilon kT/(8\pi e^2 I N_A)}$ the Debye length in cm, I the electrolyte ionic strength expressed in mol/dm^3, N_A Avogadro's number, and Y_i and Y_j are the effective surface potentials of the particles given by the following equation [35]:

$$Y_m = \frac{8\,\mathrm{tgh}\,(\bar{\psi}_m/4)}{1 + \sqrt{1 - [(2\kappa a_m + 1)/(\kappa a_m + 1)^2]\,\mathrm{tgh}^2(\bar{\psi}_m/4)}}, \quad m = i, j, \tag{4}$$

where $\bar{\psi}_m = \psi_m(e/kT)$ is the dimensionless surface potential of the particle m, and ψ_m its surface potential. The total adsorbing

particle potential is calculated using the additivity principle for the pair interactions. In this paper we always use $i = l$ in case of $i \neq j$.

Obviously, in the case of a very thin electric double layer, $\alpha = 1$, while for $\kappa a_i < 10$, it is reasonable to expect $\alpha < 0.5$ (see Appendix A). Thus, α can be considered a fitting parameter, allowing for some kind of correction for the surface interaction. As discussed in Ref. [20], in the case of monodisperse systems and thin double layers, calculating the exact value of α is not crucial, because the interparticle potential used in the model is determined mostly by the exponential term appearing in Eq. (3).

Another situation arises when the particles are asymmetric in size, as plotted in Fig. 1. Then, even at a thin double layer, the adsorbing particle attraction to the interface can result in a strong decrease of the particle–particle repulsion force. This is especially the case when the repulsion and attraction forces become comparable at some distance from the interface and so at a larger interparticle distance. Consequently, the barrier to particle adsorption in such a system is relatively low, as discussed later on. Therefore, the 2D RSA model seems to be a reasonable approximation in a system where the attractive (driving) force can be considered to be much smaller than the repulsive particle–particle force, even close to the adsorption surface, and thus corresponds to the perfect sink model. This condition is fulfilled to a reasonable extent in the case of a very low surface potential of the interface, although the problem of particle surface diffusion or adsorption reversibility can arise in such a system. If the condition is not obeyed, however, one may expect that the surface-blocking effects predicted for adsorption on precovered surfaces using the 2D RSA model can be overestimated.

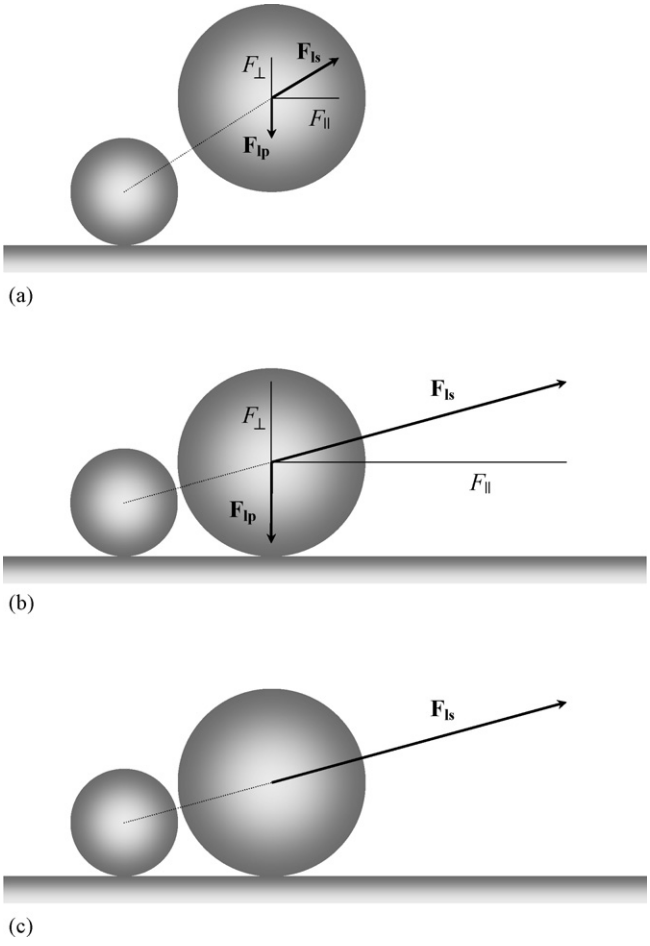

Fig. 1. Schematic representations of interaction forces acting on a large particle approaching a homogeneous interface next to a small particle: (a) $F_\perp$ and F_{lp} become comparable at some distance from the interface, the net force F_a equals $F_\parallel$ (b) $F_\perp$ and F_{lp} become comparable very close to the interface, the net force F_b equals $F_\parallel$, (c) the net force F_c equals F_{lp} according to the perfect sink model. $\mathbf{F_{ls}}$ and $\mathbf{F_{lp}}$ are the electrostatic particle–particle and particle–interface forces, respectively. $F_\parallel$ and $F_\perp$ denote the $\mathbf{F_{ls}}$ vector compounds parallel and perpendicular to the interface, respectively. Note that unlike F_a, the F_b force value is reasonably well approximated by F_c.

4. 3D model

The second RSA approach that allows electrostatic interaction, called the 3D RSA model, was proposed by Oberholzer et al. [23] and then extended to bimodal systems by Weroński [33]. Unlike the 2D model, this approach considers the particle transport from the bulk, assuming that neither electrostatic interaction nor Brownian motion causes a shift in the lateral position of the adsorbing particle as it moves toward the collector surface. During this motion, the total particle potential can be calculated according to the formula:

$$E_i(H) = \sum_{m=1}^{n} E_{ij}(H_m) + E_{ip}(H), \quad i, j = l, s, \tag{5}$$

where $H = h/a_1$ is the particle–interface gap width expressed in particle radii a_i, n the number of the small and large particles attached to the collector surface in the vicinity of the adsorbing particle, H_m the minimum surface-to-surface distance between the moving particle and the deposited particle m, E_{ij} the electrostatic (repulsive) interaction energy between them, and E_{ip} the electrostatic (attractive) interaction energy between the particle and the collector surface. The repulsive particle–particle interaction can be calculated using Eq. (3), derived from the LSA with $\alpha = 1$, and the attractive electrostatic energy between the traveling spherical particle and the adsorption surface is given by the limiting forms of Eqs. (3) and (4) when one of the particles' radii tends to infinity.

In general, a total interaction energy profile $E_i(H)$ is produced by a combination of the repulsion exerted by the particles attached at the points (X_m, Y_m), with the attraction exerted by the surface. As a consequence, the profile has a maximum E_b $(X_v, Y_v, X_1, Y_1, \ldots, X_n, Y_n)$, which represents a kinetic barrier to adsorption of the virtual particle at the point (X_v, Y_v). Its height depends on the configuration of deposited small and large particles. Using the Boltzmann distribution, one can calculate the particle adsorption probability at the given point of the adsorption surface. Fig. 2 presents the total interaction energy profiles corresponding to the simplest system, in which the large particle moves toward the surface next to the small, adsorbed particle. We assume the following parameters: $a_s = 250$ nm, $a_l = 625$ nm, $\psi_s = \psi_l = -50$ mV, $\psi_p = 100$ mV, and $I = 10^{-4}$ M. The profiles correspond to three different values of the dimensionless particle center-to-center distance projection

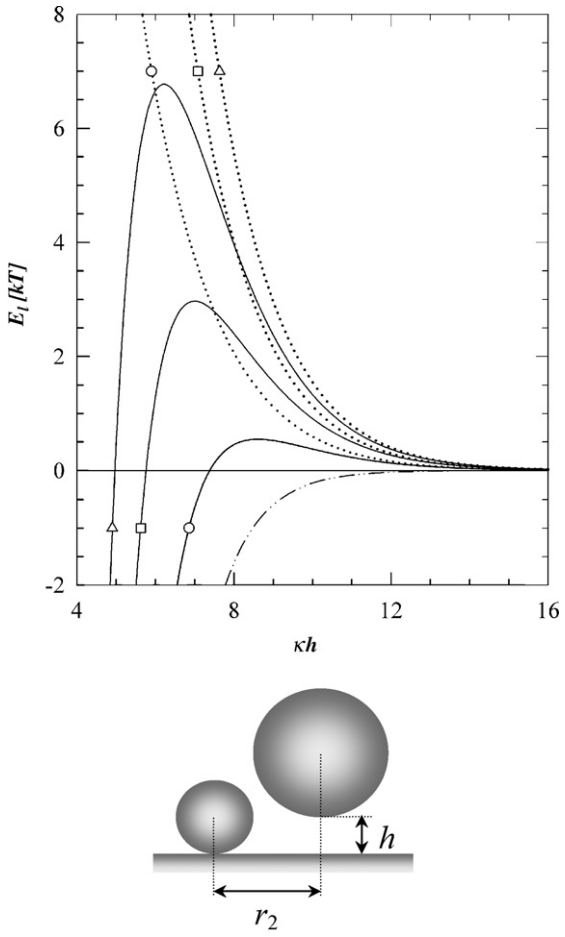

Fig. 2. Electrostatic interaction energy profiles calculated for the large particle approaching the surface next to the small particle in 3D RSA. The plots represent results based on Eq. (5). The dash-dot-dot line depicts the large particle–interface attraction. Dotted and solid lines correspond to the particle–particle repulsion and the total energy profiles, respectively. Circles, squares, and triangles indicate results obtained for $R_2 = R_0 + 2/\kappa a_l$, $R_2 = R_0 + 1.2/\kappa a_l$, and $R_2 = R_0 + 0.8/\kappa a_l$, respectively, where $R_0 = 2/\sqrt{\lambda}$. See more details in the text.

length $R_2 = r_2/a_l = \sqrt{(X_l - X_s)^2 + (Y_l - Y_s)^2}$. Based on the plots, one can conclude that the energy barrier occurs at some height above the adsorption surface and that the barrier height increases when the projection length R_2 decreases.

Although the authors of Ref. [23] claim that the 3D RSA model is more realistic, one should remember that the physics of this approach is still greatly simplified. The assumption that the particle trajectory is perpendicular to the interface seems artificial, especially for a particle overcoming the energy barrier, where the lateral component of the repulsive particle–particle force dominates. We can expect that, according to the Boltzmann distribution, most of the particles passing the energy barrier have relatively low kinetic energy (see Appendix B). More important, in the thin layer of the electrolyte adjacent to the interface, the surface forces, including the lateral particle–particle repulsion, become very large compared with the unit kT/a_i, characterizing thermal motion of the particle. Therefore, in the surface layer the particle will move approximately along the force lines of the electrostatic field. Thus, although the 3D RSA model seems to be a reasonable approach for studies of kinetic aspects of adsorption phenomena, it fails to provide appropriate monolayer structures. Consequently, one can suppose that computed jamming limits might be inaccurate as well.

5. CT model

The shortcoming of the 3D RSA model inherent in the assumption of the rectilinear trajectory of the adsorbing particle can be overcome by allowing curvilinear particle trajectory during its travel toward the adsorption surface. As discussed earlier, most of the particles passing the energy barrier move approximately along the force lines of the strong electrostatic field at the interface. The particle trajectory can be calculated according to the forces acting on the particle, starting from the point where the energy barrier was found (see Fig. 3) up to the point corresponding to the particle–interface contact. This modification delivers a new model that we will call CT RSA. In the simplest formulation of this model, the trajectory is determined assuming the mutual compensation of hydrodynamic

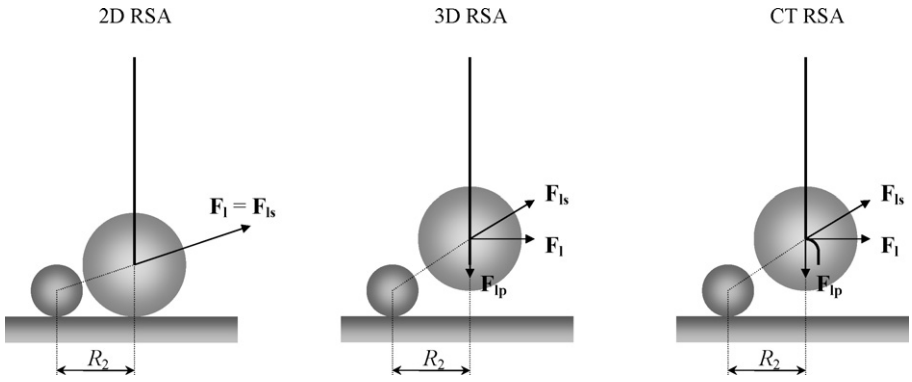

Fig. 3. Three different approaches of random sequential adsorption at precovered surfaces. Bold lines depict trajectories of the large-particle center considered in the models. The schemes show the large spherical particle at the energy barrier, where the adsorption probability is calculated, at the same distance R_2. $\mathbf{F_l}$ represents the net force acting on the particle at the barrier. Note that because of the smaller particle–particle distance in the 2D RSA model, this approach predicts much stronger repulsion than the 3D and CT models. Unlike the 3D model, the CT RSA model assumes that immediately after crossing the energy barrier, the adsorbing particle begins to move curvilinearly.

and dispersion forces between the interface and the particle approaching it. Furthermore, particle–particle hydrodynamic and dispersion interactions, external forces, and rotational motion as well as convection and Brownian motion in the thin layer are neglected. Therefore, the virtual particle trajectory can be calculated based on the deterministic equation of the motion:

$$\frac{\mathrm{d}\mathbf{R_i}}{\mathrm{d}\tau_i^*} = \mathbf{F_i}(\mathbf{R_i}), \tag{6}$$

where $\mathbf{R_i} = \mathbf{r_i}/a_i$ is the virtual-particle position vector in the a_i units, $\tau_i^* = ta_i^2/D_i^\infty$ the dimensionless time, t the time in s, $D_i^\infty = kT/6\pi\eta a_i$ the diffusion coefficient of the particle in the bulk, η the solution dynamic viscosity, and $\mathbf{F_i}$ the net force acting on the particle, expressed in the kT/a_i units and calculated according to the equation:

$$\mathbf{F_i}(\mathbf{R_i}) = -\nabla E_i(\mathbf{R_i}) \tag{7}$$

where $E_i(\mathbf{R_i})$ is the total particle potential given by Eq. (5). Note that Eq. (6) is the well-known Stokes formula relating the velocity of a spherical particle in the creeping flow to the force acting on the particle, expressed in the dimensionless form.

It should be noted that, in the CT model, the probability of particle adsorption at the final point of its trajectory is considered to be equal to the probability of the particle appearing at the energy barrier, calculated according to the Boltzmann distribution, as in the 3D model. If no energy barrier exists at the chosen virtual coordinates X_v, Y_v, the particle trajectory is not calculated. Instead, the minimum gap width H between the surface

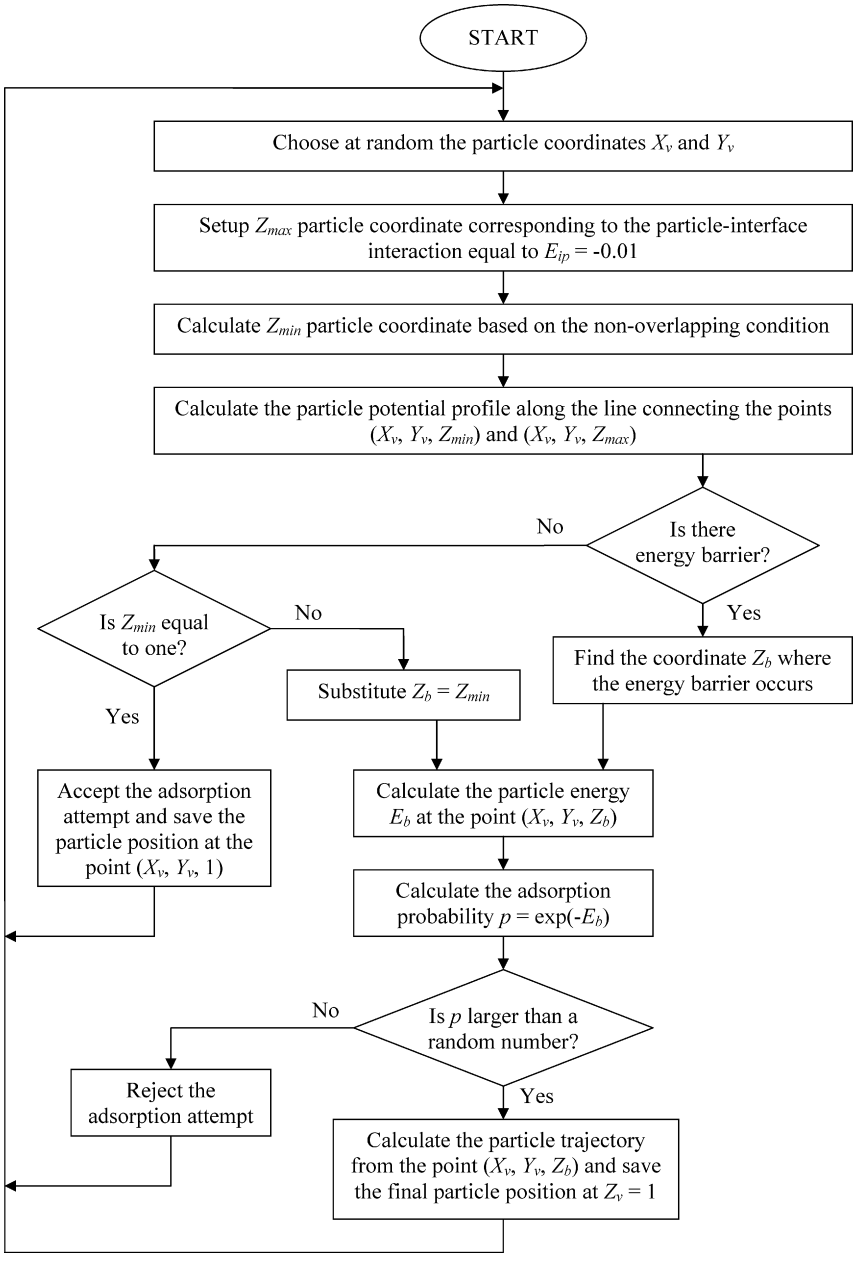

Fig. 4. Flow chart of the main simulation loop of the CT RSA model.

of the virtual particle and the interface is determined for these coordinates, under the condition of non-overlapping other, earlier adsorbed particles. If the gap width H is equal to zero, the virtual particle is adsorbed at the point (X_v, Y_v, 1), with the probability equal to one. Otherwise, the probability of particle adsorption is calculated at the point (X_v, Y_v, $H+1$), which is considered to be the starting point of the virtual-particle trajectory. The flow chart of the main simulation loop is presented in Fig. 4.

There is no conceptual difficulty in incorporating thermal motion, convection, or other types of interaction into the model, although incorporation may require some modification of the method used for choosing the particle's starting position. Eq. (6) then becomes the stochastic Langevin-type equation that is the base of the Brownian Dynamics (BD) method [36]. Therefore, using the more-sophisticated equations leads to a "smart" BD model. In spite of rapid development in computer technology, however, the computational expense of such simulations is still high, which makes the simple CT RSA model attractive and useful.

6. Analytical approximation

It is important to compare numerical results of computer simulations with analytical solutions that can be derived for special or limiting cases. Such a comparison allows verification of the used assumptions and correctness of the algorithm. Because of a lack of appropriate expressions for the available surface function in the case of the RSA of spherical particles at precovered surfaces, we have to test results of our simulations in terms of the equilibrium adsorption approach. This approach seems reasonable because the available surface functions for the RSA and equilibrium processes are indistinguishable in the early stage of deposition at low surface coverage [5]. For the equilibrium adsorption approach, we need to derive analytical formulae predicting the available surface function in equilibrium systems containing a bimodal mixture of soft spheres at an interface. We exploit the extension of the effective hard-particle approximation to bimodal systems described in Appendix C.

According to the scaled-particle theory formulated in Ref. [37] and then extended to multicomponent mixtures in Refs. [38,39], the equilibrium available surface function for the bimodal suspension of disks is given by the expression:

$$B_{id} = -\ln\left(\frac{\mu_{id}^R}{kT}\right) = (1-\theta_d)\exp\left[-\frac{3\theta_{id}+\gamma(\gamma+2)\theta_{jd}}{1-\theta_d} - \left(\frac{\theta_{id}+\gamma\theta_{jd}}{1-\theta_d}\right)^2\right], \tag{8}$$

where μ_{id}^R is the residual potential of the particles i; $i,j = l,s$; $\theta_{id} = \pi a_{id}^2 N_{id}/S$ is the disk surface coverage; a_{id} and N_{id} are the radius and number of the adsorbed disks, respectively; $\theta_d = \theta_{ld} + \theta_{sd}$, and $\gamma = a_{id}/a_{jd}$ is the disk size ratio. It should be noted that Eq. (8) describes a 2D system of hard discs only.

However, a useful approximation of the effective hard-sphere available surface function can be formulated by redefining the geometrical parameter γ. Expanding Eq. (8) in the power series of θ_{id} (up to the order of two), one obtains the following expression [28]:

$$B_{id} \cong 1 - 4\theta_{id} - (\gamma+1)^2\theta_{jd}, \tag{9}$$

which is valid for low surface coverage. In the case of the bimodal system of the effective hard spheres, it can be deduced from geometrical considerations that at low coverage, when the adsorbed particles are far apart, the large-particle available surface function is equal to:

$$B_i \cong 1 - 4\left(\frac{d_{ii}^*}{2a_i^*}\right)^2\theta_i^* - 4\lambda^*\theta_j^*, \tag{10}$$

where $\lambda = a_i/a_j$ is the spherical particle size ratio, d_{ij} the particle center-to-center distance projection length, and the asterisk indicates the effective geometrical properties. Note that the terms proportional to θ_i^* and θ_j^* represent the surface excluded because of the adsorbed particles i and j, respectively.

In the case of monodisperse systems, the last term of Eqs. (9) and (10) vanishes; therefore, in the limit of low surface coverage, the available surface functions of the small disks and spheres reduce to the well-known formulae $B_{sd} \cong 1 - 4\theta_{sd}$ and $B_s \cong 1 - 4\theta_s^*$, respectively. We used Eq. (C.7) in Appendix C to get the last formula. The formulae can be matched when $\theta_{sd} = \theta_s^*$. Taking this into account, we notice that in the case of bimodal systems, the available surface functions of the large disk and the effective large sphere – Eqs. (9) and (10), respectively – can be matched when

$$\theta_{ld} = \left(\frac{d_{ll}^*}{2a_l^*}\right)^2\theta_l^* \quad \text{and} \quad \gamma = 2\sqrt{\lambda^*} - 1. \tag{11}$$

Substituting Eqs. (C.8) through (C.11), one gets

$$\theta_{ld} = \left(\frac{d_{ll}^*}{2a_l}\right)^2\theta_l, \quad \theta_{sd} = \left(\frac{d_{ss}^*}{2a_s}\right)^2\theta_s, \quad \text{and} \quad \gamma = 2\frac{d_{ls}^*}{d_{ss}^*} - 1. \tag{12}$$

This result drives us to the conclusion that the large-sphere available surface function in the bimodal interacting spherical–particle system in the low coverage limit can be approximated by the equation:

$$B_l = (1-\theta_d)\exp\left[-\frac{3\theta_{ld}+\gamma(\gamma+2)\theta_{sd}}{1-\theta_d} - \left(\frac{\theta_{ld}+\gamma\theta_{sd}}{1-\theta_d}\right)^2\right], \tag{13}$$

where variables θ_{ld}, θ_{sd}, and γ are defined by Eqs. (12).

The limiting analytical expression for the large-particle available surface function corresponding to the initial adsorption flux of the large particles at surfaces precovered with the small ones, derived at $\theta_l = 0$, is

$$B_l^0 = (1-\theta_{sd})\exp\left[-\frac{\gamma(\gamma+2)\theta_{sd}}{1-\theta_{sd}} - \left(\frac{\gamma\theta_{sd}}{1-\theta_{sd}}\right)^2\right]. \tag{14}$$

It should be mentioned that Eqs. (13) and (14) can be interpreted as the adsorption flux only in a system where both bulk transport and the hydrodynamic scattering effect can be neglected [31].

7. Conclusion

In this paper we analyze three extended RSA models including electrostatic interaction. The simplest version of the model allowing the soft interaction is the 2D RSA model, which assumes the perfect sink particle–surface interaction and considers just the lateral particle–particle interaction. The parameter α used in the model allows some kind of correction for the particle–interface interaction. The analysis presented in the paper suggests that this model can overestimate the surface blocking effects, especially if the adsorption process is conducted at an interface partially covered with smaller preadsorbed particles. The analysis of the more-sophisticated model 3D RSA, which considers the electrostatic particle–interface interaction, suggests that the model can adequately describe the kinetic aspects of adsorption. However, because the rectilinear particle trajectory is assumed, the pair correlation function predicted by this model can be inaccurate, especially at high surface coverage. It seems that at present the best tool for studying the kinetic and structural aspects of adsorption is the CT RSA model, which includes the electrostatic particle–interface interaction and considers the curvilinear particle trajectory at a relatively low computational cost. Depending on requirements, the model can be modified to include additional effects such as external forces or convection or Brownian motion. Application of the effective hard-particle concept allows extension of the scaled-particle theory for bimodal systems of soft particles. The derived analytical formulae for the available surface function can be used for testing the numerical results in the range of low surface coverage.

Acknowledgements

The author would like to thank Prof. Z. Adamczyk for stimulating discussions and Prof. J.Y. Walz for reading the manuscript and making valuable suggestions. This work was partially supported by KBN Grant No. 3 T09A 089 27.

Appendix A

Let us accept the assumption used in Ref. [20] that the proximity of the interface does not modify the particle surface potential, and vice versa. As discussed in Ref. [20], the lateral interaction force of two (large) spherical particles at the interface can be calculated as the surface integral over the contour shown schematically in Fig. A.1 [34]:

$$\mathbf{F_{ll}} = -\int_S \left[\left(\Delta p + \frac{\varepsilon E^2}{8\pi}\right)\mathbf{n} - \frac{\varepsilon}{4\pi}(\mathbf{E}\cdot\mathbf{n})\mathbf{E}\right] \mathrm{d}S, \tag{A.1}$$

where $\Delta p \approx kTI\bar{\psi}^2$ is the osmotic pressure at a given point relative to the bulk value, $\bar{\psi} = \psi(e/kT)$ the dimensionless electric potential at this point, ψ the electric potential, $\mathbf{n}$ the unit vector normal to the closed surface S composed of the plane surfaces S_1, S_2, S_3, and S_4, and

$$\mathbf{E} = -\nabla\psi \tag{A.2}$$

the electric field strength vector. The surface integral (A.1) over S_3 is zero if the surface is drawn sufficiently far from

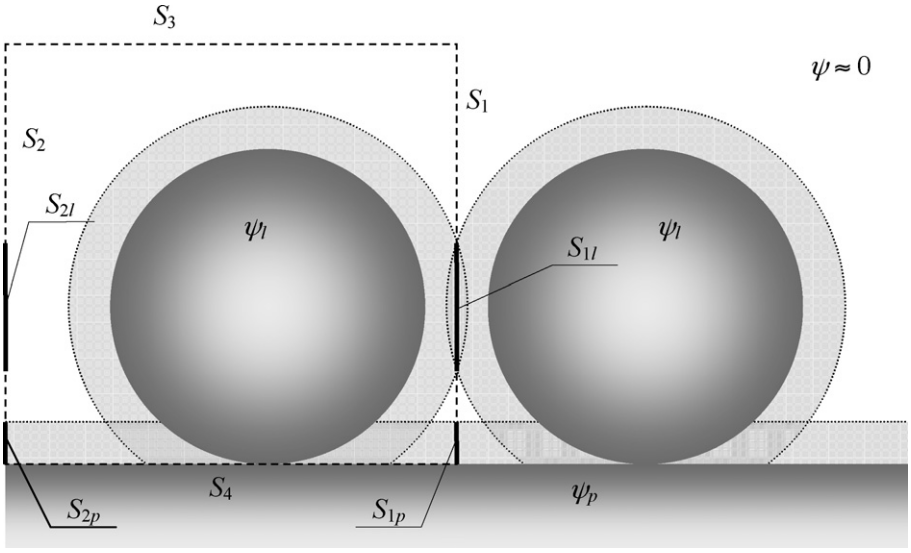

Fig. A.1. A schematic view of the electrostatic interaction of two spherical particles next to an interface at high ionic strength. The surfaces S_1, S_2, S_3, and S_4 (dashed lines) perpendicular to the plane of the picture form a close surface S around the charged spherical particle. Two surfaces parallel to the plane of the picture are not presented because their effect can always be discounted if they are chosen far enough from the particle. Dotted lines depict the borders of the area where the electric potential becomes negligible (white surface). The thickness of the double layer at the interface and at the particles is similar because it depends exponentially on the κa parameter and only linearly on the surface potential. Note that everywhere on S_3, the potential vanishes. Because of the symmetry, the force contribution from the surface S_4 is perpendicular to the interface. Bold lines depict the parts of the surfaces S_1 and S_2 over which the integration has to be conducted. Note that surfaces S_{1l} and S_{1p} are separated and that the potential on the surfaces S_{1p} and S_{2p} is identical. Therefore, the total lateral force is equal to the force acting between two isolated spherical particles with no interface.

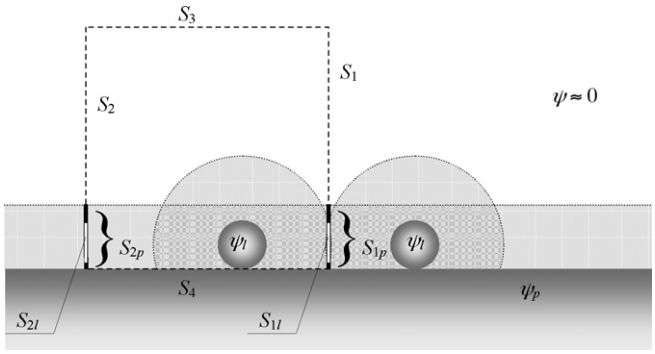

Fig. A.2. A schematic view of the electrostatic interaction of two spherical particles next to an interface at low ionic strength when the spherical electric double layers overlap very little. Bold lines (black and white) depict the parts of the surfaces S_1 and S_2 where the potential does not vanish. Due to the symmetry, the force contribution from the surface S_4 is perpendicular to the interface. Note that the potential is different only on the small parts of the surfaces S_{1p} and S_{2p}, namely on the circles S_{1l} and S_{2l}. Therefore, the integration needs to be conducted just over these surfaces. Note also that any point P on the circle S_{1l} is placed nearer the interface than the particle surface; therefore, the potential on the circle will be dominated by the contribution originating from the interface.

the interface. Moreover, if the ionic strength is high enough or if the particles' electric double layers overlap very little (see Figs. A.1 and A.2), then because of the symmetry, the surface integral over S_4 gives a perpendicular component of the force only. In these cases the lateral force can be calculated from the contributions originating from the parallel planes S_1 and S_2. It can be expressed as:

$$F_{ll}^{||} = \int_{S_1} \left[(\Delta p_1 - \Delta p_2) + \frac{\varepsilon}{8\pi}(E_{||1}^2 - E_{||2}^2) \right] \mathrm{d}S_1, \qquad \text{(A.3)}$$

where $\Delta p_i \approx kTI\bar{\psi}_i^2$, $\bar{\psi}_i$ is the osmotic pressure and the electric potential on the surface S_i, and $i = 1, 2$. $E_{||i}$ is the component of the field strength vector parallel to the surface S_i on this surface. Note that the positive value of the lateral force corresponds to the particle–particle repulsion.

According to the LSA, the electric potential $\bar{\psi}_i$ at a point P is a sum of contributions originating from the particles and the interface, which are given by the following equations:

$$\bar{\psi}^l = \frac{Y_l}{H_1 + 1} \exp[-\kappa a_l (H_1 + 1)]$$

$$\text{and} \quad \bar{\psi}^p = Y_p \exp(-\kappa a_l H), \qquad \text{(A.4)}$$

where $H_1 = h_1/a_l$ and $H = h/a_l$ are the dimensionless minimum distances between the point P and the surface of the particle and the interface, respectively. The electric potential decays rapidly (at least exponentially) with the distance from the charged surfaces. Therefore, there always exists a distance $h_{\max}$ from the particle or interface surface, at which the potential becomes negligibly small ($\psi \approx 0$, white area in Fig. A.1). Consequently, we can limit the surface integration to those parts of the surface S_1 where the potential or the field strength vector does not vanish, i.e., S_{1l} and S_{1p}, where the subscripts l and p mean the part of the surface where the potential is not equal to zero because of the particles and the interface, respectively. Also note that the distance $h_{\max}$ is relatively weakly (linearly) dependent on the surface potential. Therefore, even if the surface potential of the particle and the interface differ by a few times, the distance $h_{\max}$ from both surfaces is going to be similar.

At very high ionic strength, when the parameter κa_l is very large, the surfaces S_{1l} and S_{1p} are separated (see Fig. A.1). Then, the electric potential and the field strength on the surface S_{1p} and the corresponding surface S_{2p} are equal to the potential and field strength because of the interface alone: $\bar{\psi}_1 = \bar{\psi}_2 = \bar{\psi}^p$ and $E_{||1} = E_{||2} = E_{||p}$. Therefore, the surface integral – Eq. (A.3) – over the surface S_{1p} vanishes, and the total lateral force is equal to the surface integral over the surface S_{1l}. The potential and field strength on this surface and on the corresponding surface S_{2l} are equal to the potential and field strength because of the system of two isolated particles (with no interface in their vicinity). Therefore, the lateral interaction of the spherical particles at a very large value of the κa_l parameter can be accurately described by Eq. (3), with the parameter $\alpha = 1$. Physically, this means that at very high ionic strength, the interface has no effect on the particle–particle lateral repulsion.

At low ionic strength, when the parameter κa_l is small, the surfaces S_{1l} and S_{1p} overlap. Let us consider very weak overlapping of the spherical electric double layers first (see Fig. A.2). Then, the surfaces S_{1l} and S_{2l} are parts of the surfaces S_{1p} and S_{2p}, respectively. The electric potentials and the field strength on all the surfaces S_{1p} and S_{2p}, except the parts S_{1l} and S_{2l}, are equal: $\bar{\psi}_1 = \bar{\psi}_2 = \bar{\psi}^p$ and $E_{||1} = E_{||2} = E_{||p}$. Therefore, the only non-vanishing contribution to the integral – Eq. (A.3) – comes from the surface S_{1l}. The potential and field strength on the surface S_{1l} and on the corresponding surface S_{2l} are equal:

$$\bar{\psi}_1 = 2\bar{\psi}^l + \bar{\psi}^p,$$

$$E_{||1} = 2E_{||l} + E_{||p}, \quad \bar{\psi}_2 = \bar{\psi}^p, \quad \text{and} \quad E_{||2} = E_{||p}, \qquad \text{(A.5)}$$

respectively. Taking this into account we can express Eq. (A.3) as:

$$F_{ll}^{||} = \int_{S_1} \left[4kTI\bar{\psi}^l(\bar{\psi}^l + \bar{\psi}^p) + \frac{\varepsilon}{2\pi} E_{||l}(E_{||l} + E_{||p}) \right] \mathrm{d}S_1. \qquad \text{(A.6)}$$

As discussed in Ref. [20], $\bar{\psi}^l$ is usually of an opposite sign to $\bar{\psi}^p$ in order to ensure particle adsorption and adhesion. So are $E_{||l}$ and $E_{||p}$, because of Eq. (A.2). In the case of very weak overlapping of the electric double layers; however, the distance H_1 calculated for any point P of the surfaces S_{1l} is going to be larger (about two times on average) than the distance H. Therefore, both terms of the integrand appearing in Eq. (A.6) will be negative. Physically, this means that in the case of low ionic strength and a relatively large distance between particles at the interface, there will be a weak attraction between the particles—the lateral interaction will not diminish the particle adsorption probability at such a distance. From the perspective of the Monte Carlo simulations, this can be expressed by taking the coefficient $\alpha = 0$ in Eq. (3).

Let us next consider stronger overlapping of the particles' electric double layers (see Fig. A.3). Now, because of the potential distribution asymmetry, we also need to calculate the integral (A.1) over parts of the surface S_4, namely over the surfaces S_{41},

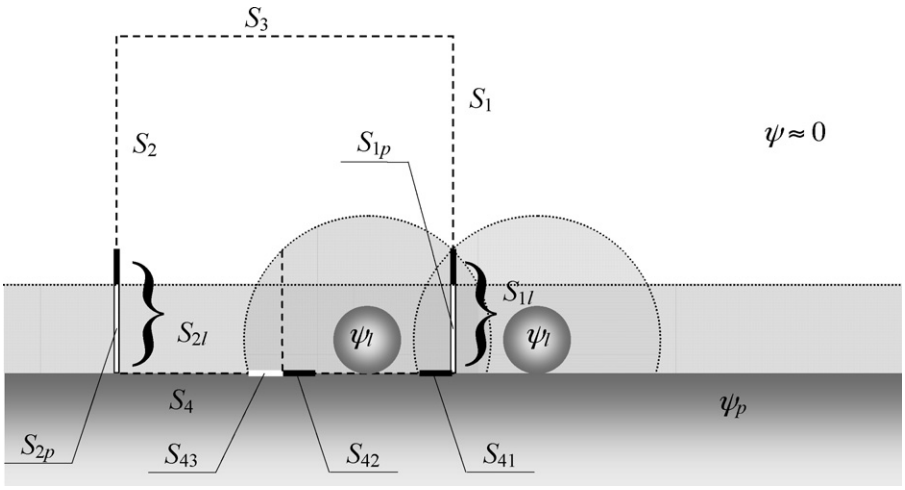

Fig. A.3. A schematic view of the electrostatic interaction of two spherical particles next to an interface at low ionic strength when overlapping of the spherical electric double layers becomes stronger. Black and white bold lines depict the parts of the surface S over which the integration has to be conducted. Note that because of the potential asymmetry at the surface S_4, we need to integrate over the identical surfaces (segments of a circle) S_{41}, S_{42}, and S_{43}, where the potential is dominated by the contribution originating from the interface. Also note that the surfaces S_{1p} and S_{1l}, as well as the surfaces S_{2p} and S_{2l}, only paratially overlap. At the particle–particle gap width about two-times larger than the distance $h_{\max}$ from the interface (like in the picture), the absolute values of the potentials $\bar{\psi}^l$ and $\bar{\psi}^p$, as well as the absolute values of the field strength $E_{||l}$ and $E_{||p}$, become comparable, and the integral (A.6) over the overlapping part of the surface S_{1l} vanishes. Then, the only non-vanishing contribution to the lateral force $F_{ll}^{||}$ comes from the part of the surface S_{1l} that does not overlap the surface S_{1p}. This part of the surface S_{1l} is a small and relatively remote segment of the large circle formed by the intersection of the two spherical electric double layers, where the potential and field strength are as in the system of two isolated particles. Therefore, the lateral force in this configuration is much smaller than a half of that between the two isolated spheres.

S_{42}, and S_{43}. Note that the three surfaces have identical shape and surface area. The lateral component of the force can originate only from the second term of the integrand appearing in Eq. (A.1). It can be expressed as:

$$F_{ll4}^{||} = \frac{\varepsilon}{4\pi}\left[\int_{S_{41}} (E_{\perp}^{p} + E_{\perp}^{l_1} + E_{\perp}^{l_2})(E_{||}^{l_1} + E_{||}^{l_2})\mathrm{d}S_{41} - \int_{S_{42}} (E_{\perp}^{p} + E_{\perp}^{l_1})E_{||}^{l_1}\mathrm{d}S_{42} - \int_{S_{43}} (E_{\perp}^{p} + E_{\perp}^{l_1})E_{||}^{l_1}\mathrm{d}S_{43}\right],$$

where the subscripts $||$ and $\perp$ mean the compounds of the field strength vectors parallel and perpendicular, respectively, to the surface S_4, and the superscripts p, l_1, and l_2 mean the contributions of the field strength vector originating from the interface, left and right particle, respectively, as they are presented in Fig. A.3. However, everywhere on the surfaces S_{41}, S_{42}, and S_{43}, we have $|E_{\perp}^{p}| \gg |E_{\perp}^{l_1}|$ and $|E_{\perp}^{p}| \gg |E_{\perp}^{l_2}|$; therefore,

$$F_{ll4}^{||} \approx \frac{\varepsilon}{4\pi}\left[\int_{S_{41}} E_{\perp}^{p}(E_{||}^{l_1} + E_{||}^{l_2})\mathrm{d}S_{41} - \int_{S_{42}} E_{\perp}^{p}E_{||}^{l_1}\mathrm{d}S_{42} - \int_{S_{43}} E_{\perp}^{p}E_{||}^{l_1}\mathrm{d}S_{43}\right],$$

and because of the symmetry

$$F_{ll4}^{||} \approx \frac{\varepsilon}{4\pi}\left[\int_{S_{41}} E_{\perp}^{p}E_{||}^{l_2}\mathrm{d}S_{41} - \int_{S_{43}} E_{\perp}^{p}E_{||}^{l_1}\mathrm{d}S_{43}\right] = 0.$$

Thus, the total lateral force $F_{ll}^{||}$ can be calculated by integration over the surface S_1 as in the case of very weak overlapping of the electric double layers. Again, the only non-vanishing contribution to the integral – Eq. (A.3) – comes from the surface S_{1l}. Note that in this configuration, the surface S_{1l} partially overlaps the surface S_{1p}. Similarly, the surface S_{2l} partially overlaps the surface S_{2p}. The potential and field strength on the overlapping parts of the surfaces S_{1l} and S_{1p}, and on the overlapping parts of the corresponding surfaces S_{2l} and S_{2p} can be expressed by Eq. (A.5). The lateral force contribution originating from this part of the surface S can be calculated according to Eq. (A.6). We can always find such a particle–particle gap width h_c (that is about two-times larger than the distance $h_{\max}$ from the interface), at which the absolute values of the potentials $\bar{\psi}^l$ and $\bar{\psi}^p$, as well as the absolute values of the field strength $E_{||l}$ and $E_{||p}$, become comparable. At this distance between the particles, the integral – Eq. (A.6) – vanishes. Then, the only non-vanishing contribution to the lateral force $F_{ll}^{||}$ comes from the part of the surface S_{1l} that does not overlap the surface S_{1p}. The potential and field strength on this part of the surface S_{1l} and on the corresponding part of the surface S_{2l} are equal to the potential and field strength because of the system of two isolated particles (with no interface in their vicinity) at the minimum surface-to-surface distance h_c. However, this part of the surface S_{1l} is only a small and relatively remote fraction of the large circle formed by the intersection of the two spherical electric double layers; therefore, the lateral force is much smaller than a half of the force acting between the two isolated spherical particles at the gap h_c. Obviously, the particle–particle potential energy, calculated by integration of the lateral force over the distance changing from infinity to h_c, will be even smaller because the non-overlapping part of the surface S_{1l} decreases with the increase of the distance between the particles and because the integral – Eq. (A.6) – over the non-overlapping part of the surface S_{1l} becomes negative at the gap wider than h_c, as discussed earlier. Therefore at the particle–particle gap width h_c, the coefficient $\alpha < 0.5$.

Note that at stronger overlapping of the spherical electric double layers, the coefficient can approach the value 0.5 or even become larger. In such a configuration, however, the particle potential energy is relatively high, and the adsorption probability, decaying exponentially with the value of the energy, becomes negligible anyhow. On the other hand, at the particle–particle gap wider than h_c, the value of the coefficient α becomes even smaller than that at the gap h_c. Therefore, if one wants to use a constant value of the coefficient in the formula (5), then the value should correspond to an average or effective value of the coefficient that is smaller than 0.5.

Appendix B

Let us consider a single central collision of a colloid particle and a high-energy solvent molecule in the bulk where the particle mobility and diffusion are isotropic. We assume that the net flow and external force acting on the particle are equal to zero and that the particle velocity after the collision is small. According to the Stokes' law, the value of the viscous force acting on the particle after the collision is equal to:

$$m_i \frac{\mathrm{d}v_i}{\mathrm{d}t} = -6\pi\eta a_i v_i(t), \quad i = s, l, \tag{B.1}$$

where $m_i = 4/3\pi a_i^3 \rho_i$ is the mass of the particle i, v_i and ρ_i are its velocity and density, respectively, and η the solution dynamic viscosity.

Integrating Eq. (B.1) once yields the velocity of the particle

$$v_i(t) = v_i(0) \exp\left(-\frac{t}{\tau}\right), \tag{B.2}$$

where $v_i(0)$ is the particle velocity at the moment of the collision, and $\tau = 2a_i^2\rho_i/9\eta$ is the characteristic time of the particle movement. For a typical colloid particle of the size on the order of 100 nm in water at room temperature, the characteristic time is on the order of 1 ns, so the particle velocity is going to decay very rapidly.

The value of the particle displacement can be calculated by integrating Eq. (B.2), which yields

$$\Delta r_i(t) = v_i(0)\tau \left[1 - \exp\left(-\frac{t}{\tau}\right)\right]. \tag{B.3}$$

Substituting

$$v_i(0) = \sqrt{\frac{3kTE_k}{2\pi a_i^3 \rho_i}}, \tag{B.4}$$

where E_k is the kinetic energy of the solvent molecule in the kT units, we can express the maximum particle displacement normalized by the particle radius as:

$$\Delta R^i_{\max} = \lim_{t\to\infty} \frac{\Delta r_i(t)}{a_i} = \sqrt{\frac{2kT\rho_i E_k}{27\pi\eta^2 a_i}}. \tag{B.5}$$

We can deduce from Eq. (B.5) that the central collision of a typical colloid particle on the order of 100 nm with a solvent molecule at kinetic energy on the order of $100kT$ results in the maximum particle displacement on the order of 1 nm—so very small. Note that the molecule kinetic energy E_k needed to move the particle by a distance of $\Delta R^i_{\max}$ increases quadratically with the value of the displacement.

The molecule kinetic energy resulting in a similar displacement of a colloid particle approaching the energy barrier at the solid-liquid interface has to be even larger than that for the collision in the bulk. This is so because the particle moving toward the energy barrier is additionally retarded because of the repulsive electrostatic interaction, as well as the hydrodynamic interaction with the adsorption surface and the adsorbed particles. According to the Boltzmann distribution, however, the probability of the collision with a high-energy solvent molecule decreases rapidly (exponentially) with the molecule kinetic energy. Therefore, as well as because of the rapid slow down of the particles moving in the solution, we can expect that the vast majority of the particles approaching the energy barriers at the adsorption surface will have a low kinetic energy.

Appendix C

If the required accuracy of computation is not very high, the modeling of the electrostatic interaction can be simplified by exploiting the effective hard-particle concept. This method, originally developed for calculating the structure of real fluids [40–43] and offering considerable advantages over the direct method of soft-particle simulation, has often been exploited for modeling colloid phenomena [20,22,44–46]. Instead of making complicated and time-consuming computations of particle energy, the effective hard-particle algorithms take into consideration a simple overlapping test in which the real geometrical particle dimensions are replaced with the effective ones. Apart from simplifying algorithms and achieving a large computational gain, the effective hard-particle approach allows comparison with analytical solutions, which are often known for hard-particle systems, and thus yields a simple test for validating numerical results. It is worthwhile to note that the algorithms are independent of the method used for calculating the effective geometrical parameters. We next discuss two methods of calculating the effective hard-particle diameter for monodisperse spherical particles and extending the effective hard-particle approach to bimodal systems.

The rigorous theoretical method of determining the relationship between the idealized hard-sphere model and the smoothly varying repulsive forces found in real fluids was developed based on the idea proposed by Zwanzig [40]. Zwanzig's idea consists in treating the intermolecular forces in a fluid as perturbations on a hard-core potential. Since then, several authors have developed various perturbation theories, introducing improved models of the effective hard particle. In our consideration, we will use the Barker-Henderson model [43]. According to this model, the dimensionless effective hard-particle diameter is equal to:

$$d^*_{ii} = a_i \int_0^\infty \{1 - \exp[-E_{ii}(R)]\}\mathrm{d}R, \quad i = s, l, \tag{C.1}$$

where $R = 2 + H_1$.

In general, the energy E_{ii} can be a complicated function of the center-to-center distance R, and the integral appearing in Eq.

(C.1) must be computed numerically. It should be mentioned that Eq. (C.1) was derived assuming short-range interactions. This approximation has been successfully applied to a description of fluids and colloidal suspensions. The model has been extended and effectively exploited for nonspherical particles as well [22].

Another, more-intuitive approach was proposed and used mostly by researchers conducting experimental studies of colloids [44–46]. Motivated by the fact that any force becomes important as soon as the work of that force is on the same order as thermal energy, some authors have chosen αkT (with $\alpha \approx 1$) as the value of the particle–particle potential at which to fix the effective hard-sphere diameter:

$$d_{ii}^* = a_i R^*, \quad E_{ii}(R^*) = \alpha. \tag{C.2}$$

The value of α has often been obtained by fitting experimental results to a hard-particle model. This method was effectively used for spheroidal particles [46] as well. As was demonstrated in Refs. [33,47], the results of the thermal energy approach are almost identical to those predicted by the Barker-Henderson model when $\alpha = 0.5$, which corresponds to the characteristic energy for one component of the 3D translation Brownian motion.

The effective hard-particle approach can easily be extended to a bimodal system. To do so, it is convenient to introduce the effective hard-particle center-to-center distance projection length, d_{ij}^*, as a generalization of the effective hard-particle diameter d_{ii}^*. Using the Barker-Henderson approximation and the 2D RSA model, one may define the lengths by the equation:

$$d_{ij}^* = a_i \int_0^\infty \{1 - \exp[-E_{ij}(R_2)]\} \mathrm{d}R_2, \quad i, j = s, l, \tag{C.3}$$

where $R_2 = \sqrt{(X_i - X_j)^2 + (Y_i - Y_j)^2} = \sqrt{R^2 - (1 - a_j/a_i)^2}$ is the dimensionless actual particle center-to-center distance projection length.

On the other hand, using the thermal-energy approximation, one has

$$d_{ij}^* = a_i R_2^*, \quad E_{ij}(R_2^*) = 0.5. \tag{C.4}$$

In the case of the 3D RSA model, Eqs. (C.3) and (C.4), involving the particle–particle energy E_{ij}, should be replaced with the equations

$$d_{ij}^* = a_i \int_0^\infty \{1 - \exp[-E_b(R_2)]\} \mathrm{d}R_2, \quad i, j = s, l, \tag{C.5}$$

and

$$d_{ij}^* = a_i R_2^*, \quad E_b(R_2^*) = 0.5, \tag{C.6}$$

respectively.

One should notice that because of a curvilinear particle trajectory in the CT RSA model, the starting and ending X_v, Y_v particle coordinates are different in general. The values obtained from Eqs. (C.5) and (C.6) correspond to the starting points of the effective particle trajectories and thus should be suitable for estimating the available surface function. On the other hand, considering the structural aspects of adsorption requires taking into account the effective final positions of the adsorbing particles. However, the main driving force acting on the particles approaching the interface is not diffusion but rather strong electrostatic attraction in the thin layer adjacent to the interface. Therefore, the equilibrium approach presented above does not seem to be reasonable for predicting the effective final particle position. Instead, we can approximate the effective final distances with the values that correspond to the effective starting positions and can be found using Eq. (6). In what follows we will use d_{ij}^* to denote the final distance-projection length corresponding to the effective starting distance.

In general, the effective hard-particle dimensions calculated using the above methods are nonadditive in the sense that the condition $d_{ls}^{*2} = d_{ll}^* d_{ss}^*$, resulting from the simple geometry of two contacting spheres on a planar surface, is not obeyed. This situation makes further analysis more complicated. Therefore,

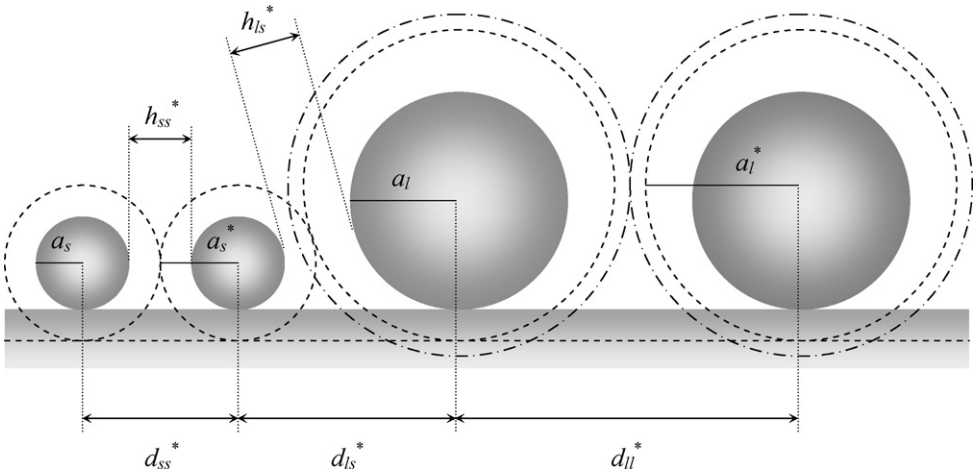

Fig. C.1. A schematic description of effective hard-small and soft-large particles at a plane interface. Dashed lines denote shapes of the effective particles and adsorption surface. Dash-dot lines show the effective interaction range of the large particles.

to ensure additivity of the effective particle dimensions, we will choose effective radii in such a way as to have the system of the small effective hard particles and the effective interacting large particles (see Fig. C.1). From the symmetry condition, we get

$$a_s^* = \frac{1}{2} d_{ss}^*, \tag{C.7}$$

and from the Pythagorean Theorem $d_{ls}^{*2} + (a_l^* - a_s^*)^2 = (a_l^* + a_s^*)^2$ we get

$$a_l^* = \frac{d_{ls}^{*2}}{4a_s^*} = \frac{d_{ls}^{*2}}{2d_{ss}^*}, \tag{C.8}$$

where variables with a star denote quantities corresponding to the effective particles.

The effective size ratio is given as:

$$\lambda^* = \frac{a_l^*}{a_s^*} = \left(\frac{d_{ls}^*}{d_{ss}^*}\right)^2 \tag{C.9}$$

(see Fig. C.2). As one can see, the increase of the interaction range results in a decrease of the effective size ratio, in agreement with intuition. Surface coverage of the effective small and large particles equals

$$\theta_s^* = \theta_s \left(\frac{a_s^*}{a_s}\right)^2 = \theta_s \left(\frac{d_{ss}^*}{2a_s}\right)^2 \tag{C.10}$$

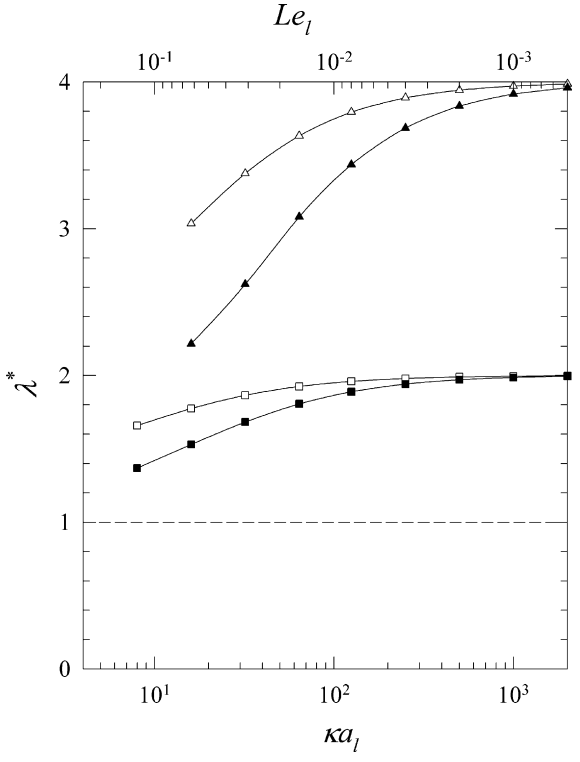

Fig. C.2. Comparison of effective particle size ratios as predicted by two models of RSA for $\lambda = 1$ (reference curve, the dashed line), $\lambda = 2$ (squares), $\lambda = 4$ (triangles). Open symbols refer to the model 2D – Eqs. (C.9) and (C.3) – and filled ones to the model 3D – Eqs. (C.9) and (C.5). The dashed line denotes identical 2D and 3D results.

and

$$\theta_l^* = \theta_l \left(\frac{a_l^*}{a_l}\right)^2 = \theta_l \left(\frac{d_{ls}^{*2}}{2a_l d_{ss}^*}\right)^2. \tag{C.11}$$

References

[1] M.Y. Boluk, T.G.M. van de Ven, Effects of polyelectrolytes on flow-induced deposition of titanium dioxide particles onto a cellophane surface, Coll. Surf. 46 (1990) 157.
[2] T.G.M. van de Ven, S.J. Kelemen, Characterizing polymers with an impinging jet, J. Coll. Interf. Sci. 181 (1996) 118.
[3] Z. Adamczyk, B. Siwek, P. Weroński, M. Zembala, Adsorption of colloid particle mixtures at interfaces, Progr. Coll. Polym. Sci. 111 (1998) 41.
[4] E.L. Hinrichsen, J. Feder, T. J(ssang, Geometry of random sequential adsorption, J. Stat. Phys. 44 (1986) 793.
[5] P. Schaaf, J. Talbot, Surface exclusion effects in adsorption processes, J. Chem. Phys. 91 (1989) 4401.
[6] J. Talbot, G. Tarjus, P. Schaaf, Unexpected asymptotic behavior in random sequential adsorption of nonspherical particles, Phys. Rev. A 40 (1989) 4808.
[7] P. Viot, G. Tarjus, Random sequential addition of unoriented squares—breakdown of Swendsen conjecture, Europhys. Lett. 13 (1990) 295.
[8] G. Tarjus, P. Viot, S.M. Ricci, J. Talbot, New analytical and numerical results on viral coefficients for 2D hard convex bodies, Mol. Phys. 73 (1991) 773.
[9] P. Viot, G. Tarjus, S.M. Ricci, J. Talbot, Random sequential adsorption of anisotropic particles. I. Jamming limit and asymptotic behavior, J. Chem. Phys. 97 (1992) 5212.
[10] S.M. Ricci, J. Talbot, G. Tarjus, P. Viot, Random sequential adsorption of anisotropic particles. II. Low coverage kinetics, J. Chem. Phys. 97 (1992) 5219.
[11] Z. Adamczyk, P. Weroński, Random sequential adsorption of spheroidal particles: kinetics and jamming limit, J. Chem. Phys. 105 (1996) 5562.
[12] P. Schaaf, A. Johner, J. Talbot, Asymptotic behavior of particle deposition, Phys. Rev. Lett. 66 (1991) 1603.
[13] B. Senger, J.-C. Voegel, P. Schaaf, A. Johner, A. Schmitt, J. Talbot, Properties of jamming configurations built up by the adsorption of Brownian particles onto solid surfaces, Phys. Rev. A 44 (1991) 6926.
[14] B. Senger, P. Schaaf, J.-C. Voegel, A. Johner, A. Schmitt, J. Talbot, Influence of bulk diffusion on the adsorption of hard spheres on a flat surface, J. Chem. Phys. 97 (1992) 3813.
[15] B. Senger, J. Talbot, P. Schaaf, A. Schmitt, J.-C. Voegel, Effect of the bulk diffusion on the jamming limit configurations for irreversible adsorption, Europhys. Lett. 21 (1993) 135.
[16] R. Jullien, P. Meakin, Random sequential adsorption with restructuring in two dimensions, J. Phys. A 25 (1992) L189.
[17] H.S. Choi, J. Talbot, G. Tarjus, P. Viot, First-layer formation in ballistic deposition of spherical particles: kinetics and structure, J. Chem. Phys. 99 (1993) 9296.
[18] G. Tarjus, P. Viot, H.S. Choi, J. Talbot, Restructuring effects in irreversible deposition of spheres on a plane, Phys. Rev. E 49 (1994) 3239.
[19] P. Schaaf, P. Wojtaszczyk, E.K. Mann, B. Senger, J.-C. Voegel, D. Bedeaux, Fluctuation of the number of adsorbed particles analyzed by a virial expansion: comparison between experiment and theory, J. Chem. Phys. 102 (1995) 5077.
[20] Z. Adamczyk, M. Zembala, B. Siwek, P. Warszyński, Structure and ordering in localized adsorption of particles, J. Coll. Interf. Sci. 140 (1990) 123.
[21] Z. Adamczyk, P. Weroński, Kinetics of irreversible adsorption of interacting spheroidal particles, Langmuir 11 (1995) 4400.
[22] Z. Adamczyk, P. Weroński, Unoriented adsorption of interacting spheroidal particles, J. Coll. Interf. Sci. 189 (1997) 348.
[23] M.R. Oberholzer, J.M. Stankovich, S.L. Carnie, D.Y.C. Chan, A.M. Lenhoff, 2D and 3D interactions in random sequential adsorption of charged particles, J. Coll. Interf. Sci. 194 (1997) 138.
[24] J. Talbot, P. Schaaf, Random sequential adsorption of mixtures, Phys. Rev. A 40 (1989) 422.

[25] P. Meakin, R. Jullien, Random-sequential adsorption of disks of different sizes, Phys. Rev. A 46 (1992) 2029.
[26] Z. Adamczyk, B. Siwek, M. Zembala, P. Weroński, Influence of polydispersity on random sequential adsorption of spherical particles, J. Coll. Interf. Sci. 185 (1997) 236.
[27] Z. Adamczyk, B. Siwek, P. Weroński, Adsorption of colloid particles at partially covered surfaces, J. Coll. Interf. Sci. 195 (1997) 261.
[28] Z. Adamczyk, P. Weroński, Random sequential adsorption on partially covered surfaces, J. Chem. Phys. 108 (1998) 9851.
[29] Z. Adamczyk, P. Weroński, E. Musiał, Irreversible adsorption of hard spheres at random site (heterogeneous) surfaces, J. Chem. Phys. 116 (2002) 4665.
[30] Z. Adamczyk, P. Weroński, E. Musiał, Colloid particle adsorption at random site (heterogeneous) surfaces, J. Coll. Interf. Sci. 248 (2002) 67.
[31] Z. Adamczyk, in: J. Toth (Ed.), Irreversible Adsorption of Particles in Adsorption: Theory, Modeling and Analysis, Marcel-Dekker, New York, 2002, p. 251.
[32] Z. Adamczyk, P. Weroński, E. Musiał, Colloid particle adsorption on partially covered (random) surfaces, J. Coll. Interf. Sci. 241 (2001) 63.
[33] P. Weroński, Kinetics of random sequential adsorption of interacting particles on partially covered surfaces, Bull. Pol. Ac. Chem. 51 (2003) 221.
[34] G.M. Bell, S. Levine, L.N. McCartney, Approximate methods of determining the double-layer free energy of interaction between two charged colloidal spheres, J. Coll. Interf. Sci. 33 (1970) 335.
[35] H. Ohshima, T.W. Healy, L.R. White, Accurate analytic expressions for the surface charge density/surface potential relationship and double-layer potential distribution for a spherical colloidal particle, J. Coll. Interf. Sci. 90 (1982) 17.
[36] M. Elimelech, J. Gregory, X. Jia, R. Williams, Particle Deposition and Aggregation: Measurement, Modelling and Simulation, Butterworth-Heinemann Ltd., Oxford, 1995, p. 224.
[37] H. Reiss, H.L. Frisch, J.L. Lebowitz, Statistical mechanics of rigid spheres, J. Chem. Phys. 31 (1959) 369.
[38] J.L. Lebowitz, E. Helfand, E. Praestgaard, Scaled particle theory of fluid mixtures, J. Chem. Phys. 43 (1965) 774.
[39] J. Talbot, X. Jin, N.H.L. Wang, New equations for multicomponent adsorption kinetics, Langmuir 10 (1994) 1663.
[40] R.W. Zwanzig, High-temperature equation of state by a perturbation method. I. Nonpolar gases, J. Chem. Phys. 22 (1954) 1420.
[41] D.A. McQuarrie, J.L. Katz, High-temperature equation of state, J. Chem. Phys. 44 (1966) 2393.
[42] J.S. Rowlinson, An equation of state of gases at high temperatures and densities, Mol. Phys. 7 (1964) 349–361;
J.S. Rowlinson, Statistical mechanics of systems with steep intermolecular potentials, Mol. Phys. 8 (1964) 107.
[43] J.A. Barker, D. Henderson, Perturbation theory and equation of state for fluids. II. A successful theory of liquids, J. Chem. Phys. 47 (1967) 4714.
[44] S.L. Brenner, A semiempirical model for the phase transition in polystyrene latexes, J. Chem. Phys. 80 (1976) 1473.
[45] A.P. Minton, H. Edelhoch, Light scattering of bovine serum albumin solutions extension of the hard particle model to allow for electrostatic repulsion, Biopolymers 21 (1982) 451.
[46] M. Piech, J.Y. Walz, Analytical expressions for calculating the depletion interaction produced by charged spheres and spheroids, Langmuir 16 (2000) 7895.
[47] P. Weroński, J.Y. Walz, An approximate method for calculating depletion and structural interactions between colloidal particles, J. Coll. Interf. Sci. 263 (2003) 327.